Advanced Composite Materials
Publication details, including instructions for authors and subscription information:
http://www.tandfonline.com/loi/tacm20

XFEM for the evaluation of elastic properties of CNT-based 3-D full five-directional braided composites

Anil Kumar Sahoo[a], I.V. Singh[a] & B.K. Mishra[a]
[a] Department of Mechanical and Industrial Engineering, Indian Institute of Technology Roorkee, Roorkee 247667, Uttarakhand, India
Published online: 09 Jan 2014.

To cite this article: Anil Kumar Sahoo, I.V. Singh & B.K. Mishra (2014) XFEM for the evaluation of elastic properties of CNT-based 3-D full five-directional braided composites, Advanced Composite Materials, 23:4, 351-373, DOI: 10.1080/09243046.2013.871173

To link to this article: http://dx.doi.org/10.1080/09243046.2013.871173

Advanced Composite Materials, 2014
Vol. 23, No. 4, 351–373, http://dx.doi.org/10.1080/09243046.2013.871173

XFEM for the evaluation of elastic properties of CNT-based 3-D full five-directional braided composites

Anil Kumar Sahoo, I.V. Singh* and B.K. Mishra

Department of Mechanical and Industrial Engineering, Indian Institute of Technology Roorkee, Roorkee 247667, Uttarakhand, India

(*Received 28 February 2012; accepted 14 August 2013*)

In the present work, a 3-D unit cell model is proposed to predict the elastic behavior of 3-D full five-directional braided composites. The model is analyzed by extended finite element method. An effective medium approximation scheme is used to evaluate the elastic properties of the composite. In the proposed unit cell model, the interface between the fiber and matrix is modeled by PU enrichment. The effects of fiber volume fraction and interior angle of braiding yarn on the elastic properties are analyzed in detail. To further enhance the elastic properties, the braided composite is enforced by randomly distributed carbon nanotubes (CNTs). A new method is proposed to evaluate the effect of CNTs on the effective properties of the composite. The present simulations show that the addition of 3% CNTs increases the effective elastic properties of 3-D braided composite nearly by 100%.

Keywords: 3-D braided composites; unit cell model; effective medium approximation (EMA); extended finite element method (XFEM); carbon nanotube (CNT)

1. Introduction

In recent years, 3-D braided composites [1,2] have been widely utilized due to their excellent mechanical properties such as good energy absorbing capability, long fatigue life, high structural integrity, high torsion stability, controllable elastic modulus, superior fracture resistance, high strength and stiffness with a corresponding low weight. Due to these properties, they have been widely used in manufacturing of engine fans for aircraft engines, thermal protection nose cone, brake block, hot-end guard tile or other parts of the motor, rocket engine throat lining, rocket nozzle, truss joint, manufacturing of compressed natural gas vase, regenerating articular cartilage, etc.

Classically, laminated composites are used when in-plane properties are of primary importance. However, they generally have poor through-thickness properties, which will cause delamination under low levels of load. To avoid these difficulties, 3-D braided composites [3] have been developed in order to improve the through-thickness behavior. 3-D braided composite is a combined product of the three-dimensional braiding technology and the advanced composite material technology.[4] As the fibers in the preform cross each other (as shown in Figure 1), the integrity of the composition is good and the drawbacks like low intensity and easy lamination between layers (as in case of laminated composites material) can be avoided.[5–7]

*Corresponding author. Email: ivsingh@gmail.com

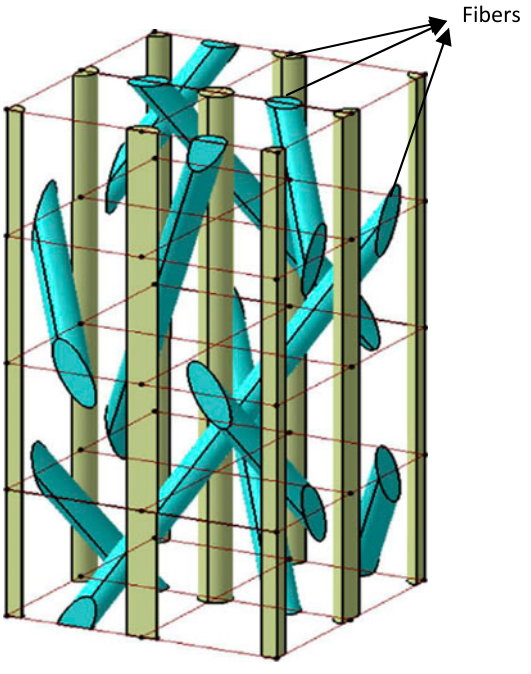

Figure 1. The preform of a 3-D braided composite.[9]

The preform construction of 3-D braided composite is divided into many types [4] such as 3-D four directions, 3-D five directions, and 3-D full five directions as shown in Figure 2. In 3-D four-directional structures, there is no axial yarn to participate in the braiding process, and in 3-D five-directional structures, there is one axial yarn (in every alternating rows and columns) passing through the pitch to form the preform whereas in 3-D full five-directional structures, there are axial yarns (in all rows and columns) passing through all the pitches.

In the past, few attempts have been made to evaluate the mechanical behavior of 3-D braided composites.[8,9] Zeng et al. [10] presented a simplified model of 3-D braided composites with transverse and longitudinal cracks. They observed that the degree of reduction in both Young's modulus and Poisson's ratio due to transverse and longitudinal cracks depends on the braid angle and the components of braided composites. Sun et al. [11] studied the influence of strain rate on the uniaxial behavior of four-step 3-D braided composite. They found that the 3-D braided composite is a kind of rate-sensitive material. The uniaxial tensile stiffness and failure stress increase with increase in strain rate, while the failure strain rate decreases. Miravete et al. [12] developed a new analytical meso-mechanical approach for 3-D braided composite based on a unit cell scheme which takes into account the geometry and the mechanical properties of both phases, i.e. the fiber and the matrix. Li et al. [13] developed a new finite element model based on the microstructure of 3-D four-directional braided composites and observed that the braiding angle is an important parameter, which affects the external dimension, braiding pitch length, and fiber volume fraction of 3-D braided composites. Dong and Feng [14] studied the strength and failure pattern of 3-D braided composites by simulating the damage propagation under tensile loading with

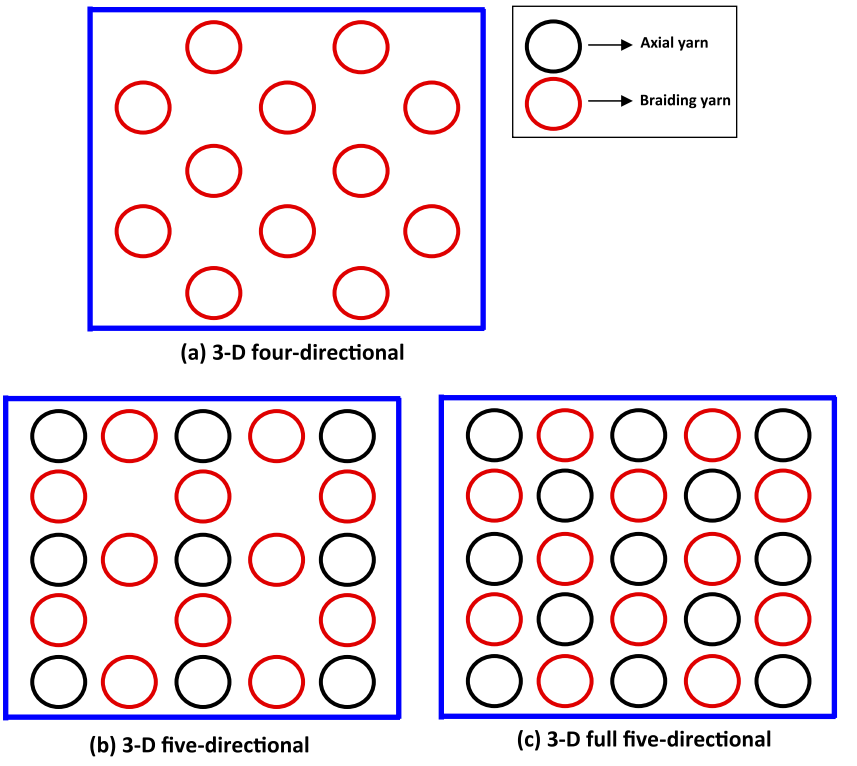

Figure 2. Preform construction of 3-D braided composite.

the help of homogenization formula of microstress. Fang et al. [15] presented a new progressive damage model for nonlinear analysis of 3-D four-directional braided composites, which is controlled by material fracture energy of the braided composites constituents and equivalent displacements.

Although the 3-D four-directional braided composites have a number of advantages over the conventional laminated composites (e.g. better out of plane stiffness, strength, high damage tolerance, etc.), but in-plane mechanical properties of 3-D four-directional composites have been relatively weakened. In order to improve in-plane properties in the predefined loading direction, 3-D five-directional braided composites had been developed by addition of uniaxial reinforced yarns in the braiding direction based on the four-step braiding patterns. There are also a few works dealing with 3-D five-directional rectangular braided composites. Xu and Xu [16] developed a new 3-D FEM for predicting the mechanical properties and the meso-scale mechanical response of 3-D five-directional braided composites. Li et al. [17] studied the mechanical properties of 3-D five-directional rectangular braided composites using finite element method. The results showed that 3-D five-directional braided composites have good mechanical properties while improved the performance along axial direction, which shows the improvement over the 3-D four-directional braided composites. The braiding angle and the fiber volume fraction were the important factors affecting the mechanical properties. Recently, Zhang et al. [18] developed a microstructural model for a 3-D full five-directional braided composite. This model shows that the fiber volume fraction can reach about 60%, which is higher than the general four-directional or five-directional

braided composites. Due to higher volume fraction, braided configuration, and straight fibers, the global property of the 3-D full five-directional braided composites can be improved.

Based on current literature, a unit cell model is proposed in the present work to predict the elastic behavior of 3-D full five-directional braided composites. First, this model is analyzed by extended finite element method (XFEM) then an effective medium approximation (EMA) approach is used to evaluate the elastic properties of the composite. To further improve the effective elastic properties of 3-D braided composite, carbon nanotube (CNTs) are added in the matrix in the form of nanoparticles as they possess extremely high stiffness, strength, and resilience and provide the ultimate reinforcing materials.[19,20] Hence, to evaluate the effective elastic properties of the CNT-based 3-D full five-directional braided composites, a multi-scale modeling approach has been utilized.

The paper is divided into five sections. Section 1 gives the introduction to the 3-D braided composite. Section 2 provides a brief overview of the XFEM formulation. Section 3 gives the details about the unit cell model (without CNTs). Section 4 gives a detailed description of the methodology followed to calculate the effective properties of 3-D full five-directional braided composites. Section 5 provides the details of the proposed CNT-based unit cell model followed by a comparison of effective elastic properties of the 3-D full five-directional braided composites with and without CNT.

2. Extended finite element method

The XFEM is a numerical technique,[21–23] which enables a local enrichment of approximation space. The enrichment is realized through the partition of unity concept. The method is useful for the approximation of the solutions with well-defined non-smooth characteristics in the small parts of the computational domain for example near discontinuities such as microfibers, holes/voids, cracks, and inclusions. To solve the problems involving discontinuities, standard finite element requires conformal meshing whereas in XFEM, these problems can be easily handled using enrichment functions without a need of conformal meshing.

2.1. *XFEM formulation*

In XFEM, enriched displacement approximation for an eight node element is given as:

$$\mathbf{u}^h = \sum_{j=1}^{8} N_j(\mathbf{x})\mathbf{u}_j + \sum_{j}^{8} g_j(\mathbf{x})\ \mathbf{a}_j \tag{1}$$

where $g_j(\mathbf{x})$ is a partition of unity-based enrichment function, defined as $g_j(\mathbf{x}) = N_j(\mathbf{x})\varphi_j(\mathbf{x})$, $\varphi(\mathbf{x}) = \pm\min\|\mathbf{x}-\mathbf{x}_\Gamma\|$, $\mathbf{x}_\Gamma$ is nearest point on the inclusion interface from a point x and N_j are the partition of unity-based finite element shape functions.

$$\begin{aligned}
u_x^h(\mathbf{x}) &= N_1(\mathbf{x})u_{1x} + N_2(\mathbf{x})u_{2x} + \cdots N_8(\mathbf{x})u_{8x} + g_1(\mathbf{x})a_{1x} + g_2(\mathbf{x})a_{2x} + \cdots g_8(\mathbf{x})a_{8x}\\
u_y^h(\mathbf{x}) &= N_1(\mathbf{x})u_{1y} + N_2(\mathbf{x})u_{2y} + \cdots + N_8(\mathbf{x})u_{8y} + g_1(\mathbf{x})a_{1y} + g_2(\mathbf{x})a_{2y} + \cdots g_8(\mathbf{x})a_{8y}\\
u_z^h(\mathbf{x}) &= N_1(\mathbf{x})u_{1z} + N_2(\mathbf{x})u_{2z} + \cdots + N_8(\mathbf{x})u_{8z} + g_1(\mathbf{x})a_{1z} + g_2(\mathbf{x})a_{2z} + \cdots g_8(\mathbf{x})a_{8z}
\end{aligned} \tag{2}$$

where u_{1x}, u_{1y}, u_{1z}, …. u_{8x},u_{8y}, u_{8z} are the unknown displacements at the nodes in x, y and z-directions, $g_1(\mathbf{x}), g_2(\mathbf{x}), \ldots g_8(\mathbf{x})$ are the enrichment terms for an element nodes defined as $g_1(\mathbf{x}) = N_1(\mathbf{x})\varphi(\mathbf{x})$, $g_2(\mathbf{x}) = N_2(\mathbf{x})\varphi(\mathbf{x}), \ldots, g_8(\mathbf{x}) = N_8(\mathbf{x})\varphi(\mathbf{x})$, and a_{1x}, a_{1y}, a_{1z},…. a_{8x}, a_{8y}, a_{8z} are additional degree of freedom corresponding to enriched nodes. $\varphi(\mathbf{x})$ is the enrichment function, which can be different for different problems. The Equation (2) can be rewritten in matrix form as

$$\mathbf{u} = [\mathbf{N} \quad \mathbf{g}]\begin{Bmatrix} \mathbf{q} \\ \mathbf{a} \end{Bmatrix} \tag{3}$$

where

$$\mathbf{u} = \begin{Bmatrix} u_x \\ u_y \\ u_z \end{Bmatrix}, \quad \mathbf{N} = \begin{Bmatrix} N_1(\mathbf{x}) & 0 & 0 & N_2(\mathbf{x}) & 0 & 0 \ldots N_8(\mathbf{x}) & 0 & 0 \\ 0 & N_1(\mathbf{x}) & 0 & 0 & N_2(\mathbf{x}) & 0 \ldots 0 & N_8(\mathbf{x}) & 0 \\ 0 & 0 & N_1(\mathbf{x}) & 0 & 0 & N_3(\mathbf{x}) \ldots 0 & 0 & N_8(\mathbf{x}) \end{Bmatrix} \tag{4a}$$

$$\mathbf{g} = \begin{Bmatrix} g_1(\mathbf{x}) & 0 & 0 & g_2(\mathbf{x}) & 0 & 0 \cdots g_8(\mathbf{x}) & 0 & 0 \\ 0 & g_1(\mathbf{x}) & 0 & 0 & g_2(\mathbf{x}) & 0 \cdots 0 & g_8(\mathbf{x}) & 0 \\ 0 & 0 & g_1(\mathbf{x}) & 0 & 0 & g_3(\mathbf{x}) \cdots 0 & 0 & g_8(\mathbf{x}) \end{Bmatrix} \tag{4b}$$

$$\mathbf{q}^T = \{u_{1x} \quad u_{1y} \quad u_{1z} \quad u_{2x} \quad u_{2y} \quad u_{2z} \cdots u_{8x} \quad u_{8y} \quad u_{8z}\} \tag{4c}$$

$$\mathbf{a}^T = \{a_{1x} \quad a_{1y} \quad a_{1z} \quad a_{2x} \quad a_{2y} \quad a_{2z} \cdots a_{8x} \quad a_{8y} \quad a_{8z}\} \tag{4d}$$

The strains at any point can be obtained as

$$\varepsilon_x = \frac{\partial u_x^h}{\partial x} = \underbrace{\frac{\partial N_1}{\partial x}u_{1x} + \frac{\partial N_2}{\partial x}u_{2x} + \cdots \frac{\partial N_8}{\partial x}u_{8x}} + \underbrace{\frac{\partial g_1}{\partial x}a_{1x} + \frac{\partial g_2}{\partial x}a_{2x} + \cdots \frac{\partial g_8}{\partial x}a_{8x}} \tag{5a}$$

$$\varepsilon_y = \frac{\partial u_y^h}{\partial y} = \underbrace{\frac{\partial N_1}{\partial y}u_{1y} + \frac{\partial N_2}{\partial y}u_{2y} + \cdots \frac{\partial N_8}{\partial y}u_{8y}} + \underbrace{\frac{\partial g_1}{\partial y}a_{1y} + \frac{\partial g_2}{\partial y}a_{2y} + \cdots \frac{\partial g_8}{\partial y}a_{8y}} \tag{5b}$$

$$\varepsilon_z = \frac{\partial u_z^h}{\partial z} = \underbrace{\frac{\partial N_1}{\partial z}u_{1z} + \frac{\partial N_2}{\partial z}u_{2z} + \cdots \frac{\partial N_8}{\partial z}u_{8z}} + \underbrace{\frac{\partial g_1}{\partial z}a_{1z} + \frac{\partial g_2}{\partial z}a_{2z} + \cdots \frac{\partial g_8}{\partial z}a_{8z}} \tag{5c}$$

The strain components in matrix form can be written as

$$\varepsilon = [\,\mathbf{B}_{\text{std}} \quad \mathbf{B}_{\text{enr}}\,]\begin{Bmatrix} \mathbf{q} \\ \mathbf{a} \end{Bmatrix} \tag{6}$$

where

$$\varepsilon = \{\,\varepsilon_x \quad \varepsilon_y \quad \varepsilon_z \quad \gamma_{xy} \quad \gamma_{yz} \quad \gamma_{zx}\,\}^T \tag{7a}$$

$$\mathbf{B}_{\text{std}} = \begin{bmatrix} \frac{\partial N_1}{\partial x} & 0 & 0 & \frac{\partial N_2}{\partial x} & 0 & 0 & \cdots & \frac{\partial N_8}{\partial x} & 0 & 0 \\ 0 & \frac{\partial N_1}{\partial y} & 0 & 0 & \frac{\partial N_2}{\partial y} & 0 & \cdots & 0 & \frac{\partial N_8}{\partial x} & 0 \\ 0 & 0 & \frac{\partial N_1}{\partial z} & 0 & 0 & \frac{\partial N_2}{\partial z} & \cdots & 0 & 0 & \frac{\partial N_8}{\partial z} \\ \frac{\partial N_1}{\partial y} & \frac{\partial N_1}{\partial x} & 0 & \frac{\partial N_1}{\partial y} & \frac{\partial N_2}{\partial x} & \cdots & \cdots & \frac{\partial N_8}{\partial y} & \frac{\partial N_8}{\partial x} & 0 \\ 0 & \frac{\partial N_1}{\partial z} & \frac{\partial N_1}{\partial y} & 0 & \frac{\partial N_2}{\partial z} & \frac{\partial N_2}{\partial y} & \cdots & 0 & \frac{\partial N_8}{\partial z} & \frac{\partial N_8}{\partial y} \\ \frac{\partial N_1}{\partial z} & 0 & \frac{\partial N_1}{\partial x} & \frac{\partial N_2}{\partial z} & 0 & \frac{\partial N_2}{\partial x} & \cdots & \frac{\partial N_8}{\partial z} & 0 & \frac{\partial N_8}{\partial x} \end{bmatrix} \tag{7b}$$

$$\mathbf{B}_{\text{enr}} = \begin{bmatrix} \frac{\partial g_1}{\partial x} & 0 & 0 & \frac{\partial g_2}{\partial x} & 0 & 0 & \cdots & \frac{\partial g_8}{\partial x} & 0 & 0 \\ 0 & \frac{\partial g_1}{\partial y} & 0 & 0 & \frac{\partial g_2}{\partial y} & 0 & \cdots & 0 & \frac{\partial g_8}{\partial x} & 0 \\ 0 & 0 & \frac{\partial g_1}{\partial z} & 0 & 0 & \frac{\partial g_2}{\partial z} & \cdots & 0 & 0 & \frac{\partial g_8}{\partial z} \\ \frac{\partial g_1}{\partial y} & \frac{\partial g_1}{\partial x} & 0 & \frac{\partial g_1}{\partial y} & \frac{\partial g_2}{\partial x} & \cdots & \cdots & \frac{\partial g_8}{\partial y} & \frac{\partial g_8}{\partial x} & 0 \\ 0 & \frac{\partial g_1}{\partial z} & \frac{\partial g_1}{\partial y} & 0 & \frac{\partial g_2}{\partial z} & \frac{\partial g_2}{\partial y} & \cdots & 0 & \frac{\partial g_8}{\partial z} & \frac{\partial g_8}{\partial y} \\ \frac{\partial g_1}{\partial z} & 0 & \frac{\partial g_1}{\partial x} & \frac{\partial g_2}{\partial z} & 0 & \frac{\partial g_2}{\partial x} & \cdots & \frac{\partial g_8}{\partial z} & 0 & \frac{\partial g_8}{\partial x} \end{bmatrix} \tag{7c}$$

Total potential energy of the system

$$\Pi^e = \frac{1}{2}\int_{V_e} \left(\varepsilon_x\sigma_x + \varepsilon_y\sigma_y + \varepsilon_z\sigma_z + \gamma_{xy}\sigma_{xy} + \gamma_{yz}\sigma_{yz} + \gamma_{zx}\sigma_{zx}\right) \mathrm{d}V - \int_{V_e} \left(uf_x + vf_y + wf_z\right) \mathrm{d}V - \cdots \int_{\Omega_e} \left(ut_x + vt_y + wt_z\right) \mathrm{d}\Omega - \sum_{i=1}^{8} \left(u_i P_{ix} + v_i P_{iy} + w_i P_{iz}\right) \tag{8}$$

$$\Pi^e = \frac{1}{2}\int_{V_e} \boldsymbol{\varepsilon}^T \boldsymbol{\sigma}\, \mathrm{d}V - \int_{V_e} \mathbf{u}^T \mathbf{f}\, \mathrm{d}V - \int_{\Omega_e} \mathbf{u}^T \mathbf{t}\, \mathrm{d}\Omega - \mathbf{q}^T \mathbf{P} \tag{9}$$

$$\Pi^e = \frac{1}{2}\int_{\Omega_e} \boldsymbol{\varepsilon}^T \mathbf{D}\, \boldsymbol{\varepsilon}\, h\, \mathrm{d}A - \int_{\Omega_e} \mathbf{u}^T \mathbf{f}\, h\, \mathrm{d}A - \int_{\Gamma_e} \mathbf{u}^T \mathbf{t}\, h\, \mathrm{d}\Gamma - \begin{bmatrix}\mathbf{q}^T & \mathbf{a}^T\end{bmatrix} \{\tilde{\mathbf{P}}\} \tag{10}$$

$$\Pi^e = \frac{1}{2}\begin{bmatrix}\mathbf{q}^T & \mathbf{a}^T\end{bmatrix} \underbrace{\int_{\Omega_e} \begin{Bmatrix} \mathbf{B}_{\text{std}}^T \\ \mathbf{B}_{\text{enr}}^T \end{Bmatrix} \mathbf{D} [\mathbf{B}_{\text{std}} \quad \mathbf{B}_{\text{enr}}] h\, \mathrm{d}A}_{\tilde{\mathbf{K}}} \begin{Bmatrix} \mathbf{q} \\ \mathbf{a} \end{Bmatrix} - \begin{bmatrix}\mathbf{q}^T & \mathbf{a}^T\end{bmatrix} \underbrace{\int_{\Omega e} \begin{bmatrix} \mathbf{N}^T \\ \mathbf{g}^T \end{bmatrix} \begin{Bmatrix} f_x \\ f_y \\ f_z \end{Bmatrix} h\, \mathrm{d}A}_{\tilde{\mathbf{F}}b} - \begin{bmatrix}\mathbf{q}^T & \mathbf{a}^T\end{bmatrix} \underbrace{\int_{\Gamma} e \begin{bmatrix} \mathbf{N}^T \\ \mathbf{g}^T \end{bmatrix} \begin{Bmatrix} t_x \\ t_y \\ t_z \end{Bmatrix} d\Gamma}_{\tilde{\mathbf{F}}t} - \begin{bmatrix}\mathbf{q}^T & \mathbf{a}^T\end{bmatrix} \{\tilde{\mathbf{P}}\} \tag{11}$$

$$\Pi^e = \frac{1}{2}[\mathbf{q}^T \quad \mathbf{a}^T] \tilde{\mathbf{K}} \begin{Bmatrix} \mathbf{q} \\ \mathbf{a} \end{Bmatrix} - [\mathbf{q}^T \quad \mathbf{a}^T]\{\tilde{\mathbf{F}}_b\} - [\mathbf{q}^T \quad \mathbf{a}^T]\{\tilde{\mathbf{F}}_t\} - [\mathbf{q}^T \quad \mathbf{a}^T]\{\tilde{\mathbf{P}}\} \tag{12}$$

Minimizing the potential energy with respect to unknowns of the elemental equations, i.e. $u_1x, u_1y, u_1z, u_2x, u_2y, u_2z, \ldots a_8x, a_8y$ and a_8z, we obtain

$$[\tilde{\mathbf{K}}] \begin{Bmatrix} \mathbf{q} \\ \mathbf{a} \end{Bmatrix} = \{\tilde{\mathbf{F}}_b\} + \{\tilde{\mathbf{F}}_t\} + \{\tilde{\mathbf{P}}\} \tag{13}$$

or

$$[\tilde{\mathbf{K}}]\{\mathbf{U}\} = \{\mathbf{F}\} \tag{14}$$

where

$$[\tilde{\mathbf{K}}] = \begin{bmatrix} \mathbf{K}_{uu} & \mathbf{K}_{ua} \\ \mathbf{K}_{au} & \mathbf{K}_{aa} \end{bmatrix} \tag{15}$$

$$\mathbf{K}_{uu} = \int_{\Omega_e} \mathbf{B}_{\text{std}}^T \mathbf{D}\, \mathbf{B}_{\text{std}}\, h\, \mathrm{d}A \tag{16a}$$

$$\mathbf{K}_{ua} = \int_{\Omega_e} \mathbf{B}_{\text{std}}^T \mathbf{D}\, \mathbf{B}_{\text{enr}} h\, \mathrm{d}A \tag{16b}$$

$$\mathbf{K}_{au} = \mathbf{K}_{ua}^T \tag{16c}$$

$$\mathbf{K}_{aa} = \int_{\Omega_e} \mathbf{B}_{\text{enr}}^T \mathbf{D} \mathbf{B}_{\text{enr}} h\, \mathrm{d}A \tag{16d}$$

$$\mathbf{F}_b = \int_{\Omega_e} \begin{bmatrix} \boldsymbol{\psi}^T \\ \mathbf{g}^T \end{bmatrix} \begin{Bmatrix} f_x \\ f_y \\ f_y \end{Bmatrix} h\, \mathrm{d}A \tag{16e}$$

$$\mathbf{F}_t = \int_{\Gamma_e} \begin{bmatrix} \mathbf{N}^T \\ \mathbf{g}^T \end{bmatrix} \begin{Bmatrix} t_x \\ t_y \\ t_z \end{Bmatrix} h\, \mathrm{d}\Gamma \tag{16f}$$

$$\{\mathbf{F}_c\} = \begin{Bmatrix} P_{1x} & P_{1y} & P_{1z} & P_{2x} & P_{2y} & P_{2z} \cdots P_{8x} & P_{8y} & P_{8z} & 0 & 0 & 0 \end{Bmatrix} \tag{16 g}$$

2.2. *XFEM Implementation*

There is no considerable difference in the implementation of finite element method and XFEM. The FEM methodology essentially consists of

- Definition of geometry, i.e. nodes and their connectivity.
- Computation of shape functions and their derivatives.
- Assembly procedure for generating stiffness matrix K.
- Integration of weak form using Gauss quadrature.
- Imposing essential boundary conditions.
- Solution of equations to get nodal displacements.
- Post-processing (Evaluation of stresses and strains).

General XFEM procedure for writing the MATLAB code is given below:

(i) Define geometry and generate the nodes.
(ii) Define material properties along with the level set function for the inclusions (fibers).
(iii) Generate the connectivity matrix.

(iv) Identify the split elements as per the level sets.
(v) Add fictitious nodes for split nodes, i.e. one for each split node (three extra degrees of freedoms in 3-D domain).
(vi) Define the assembly algorithm to take care of additional nodes (fictitious nodes).
(vii) Generate the Gauss points for split and normal elements. In the split elements, the higher order Gauss quadrature is used by sub-triangulation approach.
(viii) Integrate over elements for calculating B-matrix consisting of shape function derivatives.
(ix) Integrate along the traction boundary using first-order Gauss quadrature to form the nodal force vector f.
(x) Apply essential boundary conditions to obtain the displacement vector u.
(xi) Solve for displacement and fictitious degrees of freedoms.
(xii) Extract the nodal displacements excluding the fictitious degrees of freedoms.
(xiii) Calculate stresses and strains.
(xiv) Plot the stress and strain contours.

3. Unit cell model (without CNTs)

A unit cell is defined as a cell or a building block of the composite. It is also called a representative volume element (RVE). A unit cell as the name suggests describes a unit portion of a composite material, which when stacked together in rows and columns will form the actual composite structure. For example, a unit cell of a simple particulate composite is a cube with a spherical particle at the center. A unit cell model is defined in terms of the microstructural parameters including volume fractions, connectivity, and anisotropic spatial distribution of phases. One of the key issues in estimation of the effective constitutive relation of a composite is the appropriate modeling of the stress transfer relation of the constituent phases with specific microstructures.

In this paper, a unit cell model having the structure of 3-D full five directions is shown in Figure 3, where a, b, and c are width, thickness, and height of the unit cell, respectively. An interior angle is the angle between central axis of the braiding yarn and Z_0 axis. For the geometrical modeling of the unit cell, the braiding and axial yarns are assumed to be straight and circular cross-sections of same diameters. Under these assumptions, the final position of each in the unit cell can be selected as shown in Figure 4. To prepare a finite element model of the unit cell for further analysis, the size of the unit cell (Figure 3) is taken as per Table 1.

In the present work, the 3-D full five-directional braided composite has been modeled as shown in Figure 5. An algorithm is developed to simulate the dynamics of 3-D full five-directional braided composites so that one can understand and design new composites with an ease. The fibers in the microstructure are assumed as 3-D solid cylindrical inclusions. The matrix and the reinforcement along with the homogenous medium approximate the intertwining structure of the 3-D braided composite. The radius of each fiber is determined using fiber volume fraction. The following relation is used to calculate the radius of the fiber:

$$V_f = \frac{V_y}{V} \tag{17}$$

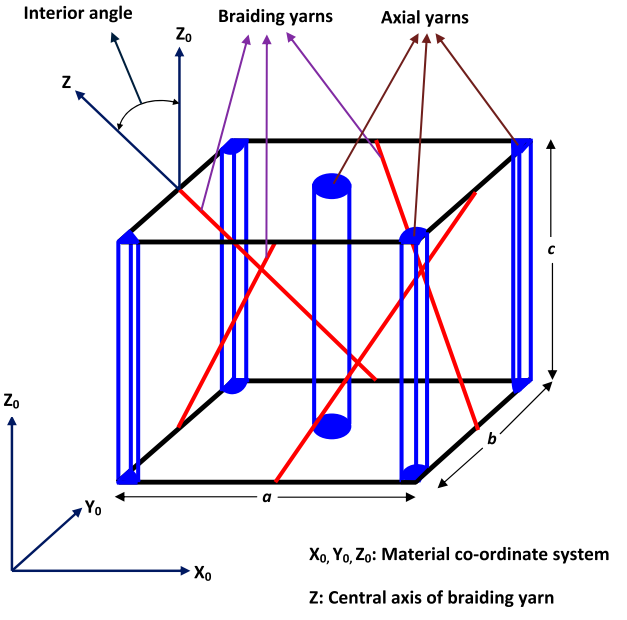

Figure 3. Schematic illustration of the fiber structure of 3-D full five-directional braided composites.

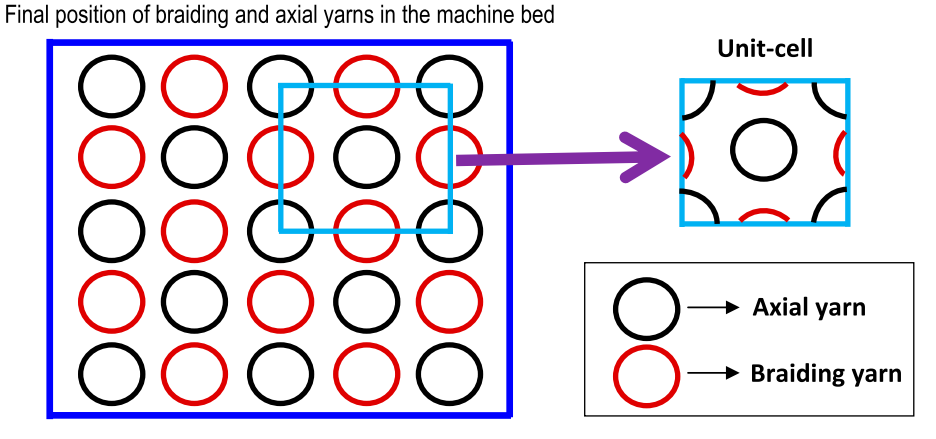

Figure 4. Selection of the unit cell of 3-D full five-directional braided composites.

Table 1. Dimension of unit cell.

Parameters	Value
Width (*a*)	20 mm
Thickness (*b*)	20 mm
Height (*c*)	20 mm
Interior angle	35.6°

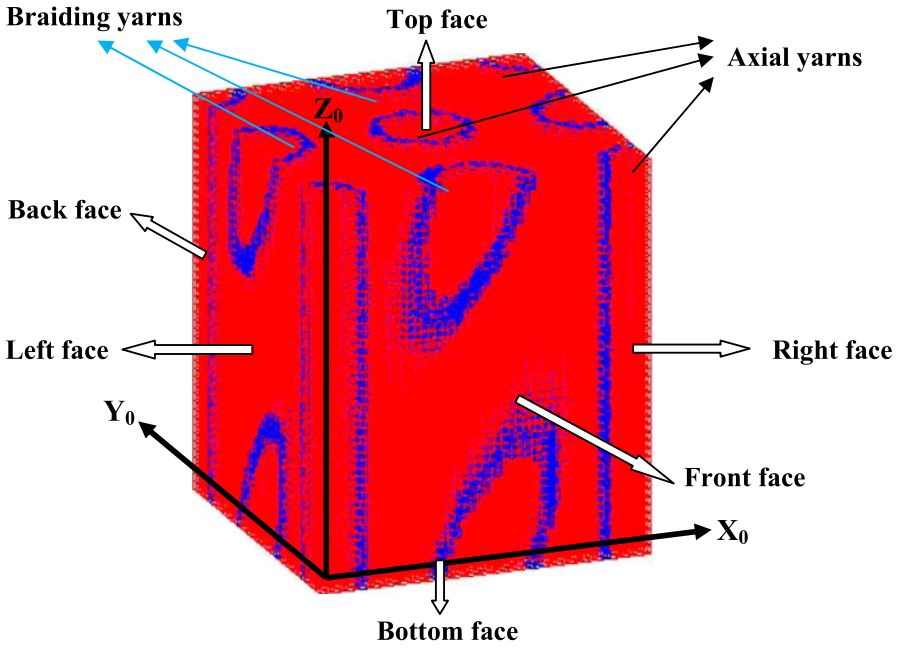

Figure 5. Unit cell model for 3-D full five-directional braided composite.

where V_f is the fiber volume fraction, V_y is the total volume of the yarns (axial and braiding) = $n \times (\pi r^2 h)$, V is the volume of the unit cell, r is radius of the fiber, h is the height of the fiber, and n is number of fibers in the unit cell. The fibers are used to form nine level set values for each node in the domain. These values are the normal distances from the boundary,[24] and are given by

$$\psi(X_0, Y_0, Z_0) = \sqrt{x^2 + y^2 + z^2} - r_c \tag{18}$$

where x, y, $z$are co-ordinates of center of the cylindrical inclusion (fiber), r_c is the radius of the solid cylinder (fiber), and ψ is level set function and is equal to zero on the circumference of the cylinder (fiber).

4. Effective medium approximation

It has been noticed that the different 3-D braided composites show different mechanical properties depending on the volume fraction, ratios of elastic modulus, interior angle, geometry, etc. Thus, homogenization of these composite is very important to analyze and characterize their mechanical behavior. The EMA suggests that an equivalent homogenous medium can be found out, which will have properties similar to that of composite, i.e. by replacing the actual heterogeneous composite by an equivalent homogeneous material. This homogenous material is an idealization but is an essential approximation for the further analysis of the composite, which otherwise is very difficult to analyze. In past, many researchers have used EMA approach to evaluate the effective properties of the composites. In fact, the study of composite materials involves the finding of the effective properties such as Young's modulus, shear modulus, and Poisson's ratio. Thus, EMA is very relevant and useful technique to find out the

effective properties of a composite. There are various methods by which one can find a homogenous material to mimic the properties of the composite material. To approximate a medium, first find that property which influences the overall property. For example, volume fraction is the most important factor, which influences a composite material. Other factors like geometry, interior angle, and temperature also affect the overall properties of the composite.

In the present work, 3-D full five-directional braided composite has been solved using XFEM and analyzed by EMA. This composite shows a transversely isotropic behavior at macroscopic level due to the orientation of the fibers in the composite. In this composite, both the matrix and the fibers are assumed to be isotropic in nature. A homogenization approach is used to obtain the effective elastic properties of 3-D full five-directional braided composites by considering the heterogeneous behavior at microscale and homogeneous behavior at macroscale.[16]

In general, the global strain–stress relation can be written as

$$\bar{\varepsilon}_i = S_{ij}\bar{\sigma}_j \tag{19}$$

where S_{ij} is the effective compliance matrix. Assuming a set of the global stress, $\bar{\sigma}_{ij}$ and applying the essential boundary conditions given in Table 2, one can obtain a strain distribution in the RVE. Then, the global strain, $\bar{\varepsilon}_{ij}$ corresponding to global stress can be obtained by $\bar{\varepsilon}_{ij} = \frac{1}{V}\int_V \varepsilon_{ij} dV$ where V is the volume of the unit cell.

The boundary conditions, u_x, u_y, and u_z denote the displacements in X_0, Y_0 direction, and Z_0 directions, respectively. Thus, by applying six components of $\bar{\sigma}_{ij}$ as presented in Table 3, six equations are obtained. By assigning the six sets of the global stress, $\bar{\sigma}_{ij}^k \cdot (k = 1, 2 \ldots 6)$, the corresponding global strain $\bar{\varepsilon}_{ij}^k$ can be calculated using the following equations

Table 2. Boundary condition for calculation of effective elastic properties of the unit cell.

Cases	Properties	Essential boundary condition	Natural boundary condition
1	E_x	$u_x = 0$ (on left face), $u_y = 0$ (on front & back face), $u_z = 0$ (on bottom & top face),	Axial stress along X_0 (on right face)
2	E_y	$u_x = 0$ (on left & right face), $u_y = 0$ (on back face), $u_z = 0$ (on bottom & top face),	Axial stress along Y_0 (on front face)
3	E_z	$u_x = 0$ (on left & right face), $u_y = 0$ (on front & back face), $u_z = 0$ (on bottom face),	Axial stress along Z_0 (on top face)
4	G_{xz}	$u_x = u_y = 0$ (on bottom & top face), $u_x = u_z = 0$ (on back face), $u_x = 0$ (on front face), $u_y = u_z = 0$ (on left & right face),	Shear stress along Z_0 (on front face)
5	G_{yz}	$u_x = u_y = 0$ (on bottom & top face), $u_x = u_z = 0$ (on front & back face), $u_y = u_z = 0$ (on left face), $u_z = 0$ (on right face),	Shear stress along Y_0 (on right face)
6	G_{xy}	$u_x = u_y = 0$ (on bottom face), $u_y = 0$ (on top face), $u_x = u_z = 0$ (on front & back face), $u_y = u_z = 0$ (on left & right face),	Shear stress along X_0 (on top face)

Table 3. Loading case of natural boundary condition.

K	$\bar{\sigma}_x(N)$	$\bar{\sigma}_y(N)$	$\bar{\sigma}_z(N)$	$\bar{\tau}_{xz}(N)$	$\bar{\tau}_{yz}(N)$	$\bar{\tau}_{xy}(N)$
1	100	0	0	0	0	0
2	0	100	0	0	0	0
3	0	0	100	0	0	0
4	0	0	0	100	0	0
5	0	0	0	0	100	0
6	0	0	0	0	0	100

$$\left\{\bar{\varepsilon}_i^1, \bar{\varepsilon}_i^2, \ldots, \bar{\varepsilon}_i^5, \bar{\varepsilon}_i^6\right\} = S_{ij}\left\{\bar{\sigma}_j^1, \bar{\sigma}_j^2, \ldots, \bar{\sigma}_j^5, \bar{\sigma}_j^6\right\} \tag{20}$$

Hence, by solving the above equations, one can directly obtain the effective compliance matrix S_{ij} in the following form:

$$S_{ij} = \begin{bmatrix} \frac{1}{E_x} & -\frac{v_{xy}}{E_y} & -\frac{v_{xz}}{E_z} & 0 & 0 & 0 \\ -\frac{v_{yx}}{E_x} & \frac{1}{E_y} & -\frac{v_{yz}}{E_z} & 0 & 0 & 0 \\ -\frac{v_{zx}}{E_x} & -\frac{v_{zy}}{E_y} & \frac{1}{E_z} & 0 & 0 & 0 \\ 0 & 0 & 0 & \frac{1}{G_{xz}} & 0 & 0 \\ 0 & 0 & 0 & 0 & \frac{1}{G_{yz}} & 0 \\ 0 & 0 & 0 & 0 & 0 & \frac{1}{G_{xy}} \end{bmatrix} \tag{21}$$

4.1. *Results and discussion*

The elastic properties of constituents of the composite in the unit cell are listed in Table 4. The fiber volume fraction of yarn is assumed to be 45% in the model. The XFEM mesh for the unit cell (Figure 5) consists of 8000 nodes and 6859 eight-nodded brick elements.

After assigning the mechanical properties to the components, the effective compliance matrix of the 3-D full five-directional braided composite is evaluated as follows:

$$S_{ij} = \begin{bmatrix} 0.0310 & -0.0093 & -0.0063 & 0 & 0 & 0 \\ -0.0093 & 0.0310 & -0.0063 & 0 & 0 & 0 \\ -0.0063 & -0.0063 & 0.0211 & 0 & 0 & 0 \\ 0 & 0 & 0 & 0.0685 & 0 & 0 \\ 0 & 0 & 0 & 0 & 0.0685 & 0 \\ 0 & 0 & 0 & 0 & 0 & 0.0807 \end{bmatrix}_{GPa^{-1}} \tag{22}$$

Table 4. Mechanical properties of component materials.

Materials	Young's modulus E, GPa	Poisson's ratio(v)
Carbon fiber T300	221	0.3
Epoxy resin	4.5	0.3

It is noted that relatively fine mesh is required in order to obtain more accurate stress distribution, especially near the boundaries of the RVE.

According to the relationship between the elastic constants and the compliance matrix S_{ij}, nine independent elastic constants of 3-D full five-directional braided composites can be calculated by the following relations $E_x = \frac{1}{S_{11}}$, $E_y = \frac{1}{S_{22}}$, $E_z = \frac{1}{S_{33}}$, $v_{xy} = -\frac{S_{12}}{S_{22}}$, $v_{xz} = -\frac{S_{13}}{S_{33}}$, $v_{yz} = -\frac{S_{23}}{S_{33}}$, $G_{xz} = \frac{1}{S_{44}}$, $G_{yz} = \frac{1}{S_{55}}$, and $G_{xy} = \frac{1}{S_{66}}$. The results obtained by XFEM using unit cell model are presented in Table 5.

The unit cell of 3-D full five-directional braided composites produced by the four-step 1×1 rectangular braiding procedure (Figure 4) is shown in Figure 5. The effect of fiber volume fraction on the effective elastic properties of 3-D full five-directional braided composites is studied. The upper bound and lower bound of the unit cell for a particular fiber volume fraction can be calculated using the rule of mixture as given below:

$$E_u = (V_f \times E_f) + (V_m \times E_m) \tag{23}$$

$$E_l = \frac{E_f \times E_m}{(V_f \times E_m) + (V_m \times E_f)} \tag{24}$$

where E_u is the upper bound (axial modulus) of composite, E_l is the lower bound (transverse modulus) of composite, E_f is the elastic modulus of fiber (Carbon), E_m is the elastic modulus of matrix (Epoxy), V_f is the fiber volume fraction in the unit cell, and V_m is the matrix volume fraction in the unit cell.

Figure 6 describes the variation of E_z with the fiber volume fraction. This figure shows that the elastic modulus E_z increases sharply with the increase in fiber volume fraction and lies within the theoretical bounds, i.e. upper and lower bounds calculated by Equations (23) and (24). Figure 7 presents the variation of elastic moduli $E_x (= E_y)$ with the fiber volume fraction. These results show that with the increase in fiber volume fraction, the elastic modulus E_x also increases. Figures 8 and 9 show the variation of the shear modulus, G_{xy} and G_{xz} ($G_{xz} = G_{yz}$) with the fiber volume fraction. From the results presented in these figures, it is seen that shear moduli increase monotonically with the increase in fiber volume fraction. The values of Poisson's ratio for both the matrix and fibers are taken as 0.3; therefore, effective values of v_{xy}, v_{yz}, and v_{xz} are found nearly same, i.e. 0.3. Figure 10 shows that the elastic modulus E_z decreases with the increase in the interior angle. Figure 11 shows that the elastic moduli E_x and E_y ($E_x = E_y$) increase with the increase in the interior angle. Figure 12 shows the plots of maximum principal stress components for the unit cell subjected to loading given in case-3 of Table 2. From these results, it is found that the stresses in yarns (fibers) are more than in the matrix region.

5. Proposed CNT-based unit cell model

To further enhance the properties, CNTs are added in 3-D full five-directional braided composites. At nanoscale, the stresses and strains are governed by different physics of

Table 5. Effective elastic constants predicted by XFEM.

Young's modulus (GPa)			Shear modulus (GPa)			Poisson's ratio		
E_x	E_y	E_z	G_{xz}	G_{yz}	G_{xy}	v_{xz}	v_{yz}	v_{xy}
32.21	32.21	47.39	14.60	14.60	12.39	0.3	0.3	0.3

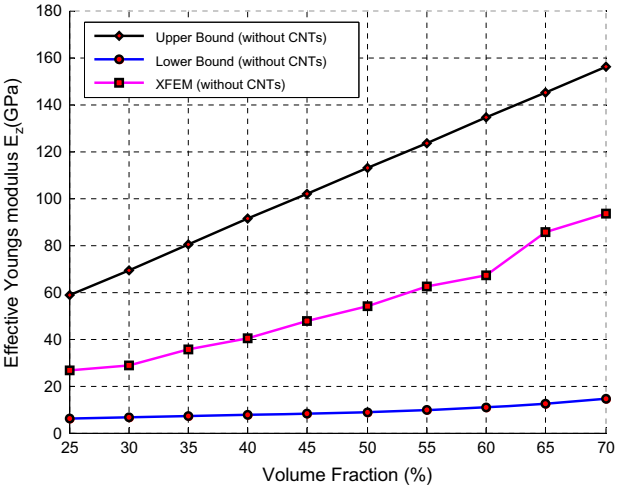

Figure 6. A plot of effective Young's modulus E_z with the fiber volume fraction.

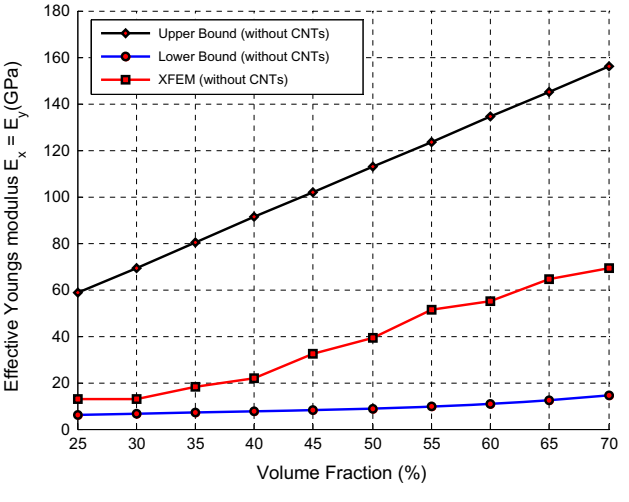

Figure 7. A plot of effective Young's modulus E_x and E_y ($E_x = E_y$) with the fiber volume fraction.

the material. Hence, the continuum mechanics-based finite element approach cannot be used successfully for the simulation of CNT-composite until the physics of nanoscale is incorporated in the continuum model. To cope-up with this, in the present work, a microscale unit cell model has been proposed. At microscale, the nanotubes can be treated as particles or points.

As explained in the above paragraph, the nanotubes are represented by particles or points. In proposed approach, the CNT properties are given to some randomly selected Gauss points (integration points for finite element analysis) in the domain. There are two procedures to evaluate the effective properties of the braided composite. One procedure to calculate the effective properties of CNT-based 3-D full five-directional braided composite is summarized as follows (see Figure 13):

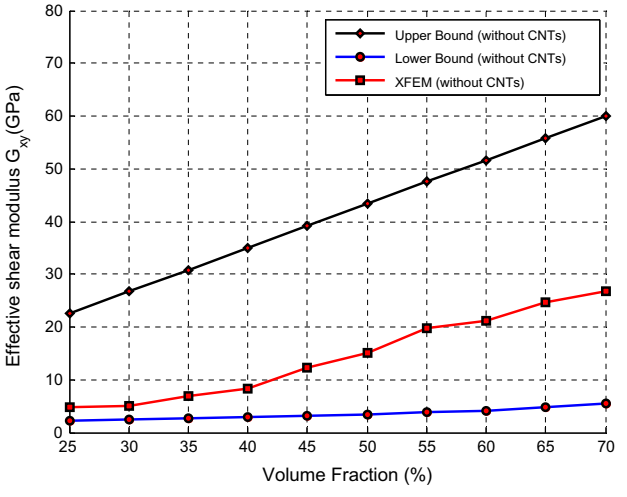

Figure 8. A plot of effective shear modulus G_{xy} with the fiber volume fraction.

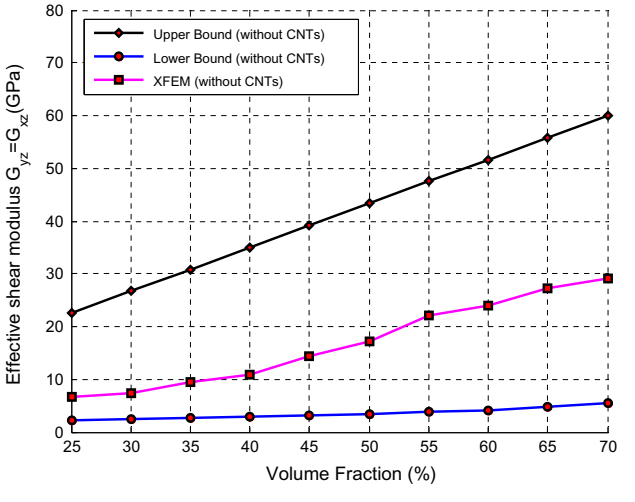

Figure 9. A plot of effective shear modulus G_{yz} and G_{xz} with the fiber volume fraction.

(i) Model the unit cell according to the given geometry.
(ii) Generate the Gauss points inside the problem domain.
(iii) Calculate the total number of Gauss points in the unit cell, and randomly select 3% of total Gauss points in the following directions:
- 1% in X_0 direction.
- 1% in Y_0 direction.
- 1% in Z_0 direction.

(i) Give the properties of CNT to 3% Gauss points, and properties of the matrix to the rest of the Gauss points.
(ii) Evaluate the effective properties of the unit cell by applying the EMA and boundary conditions as shown in Table 2.

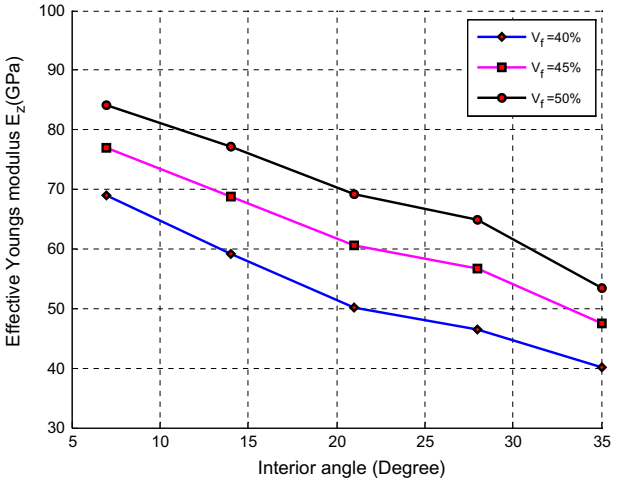

Figure 10. A plot of effective elastic modulus E_z with the interior angle.

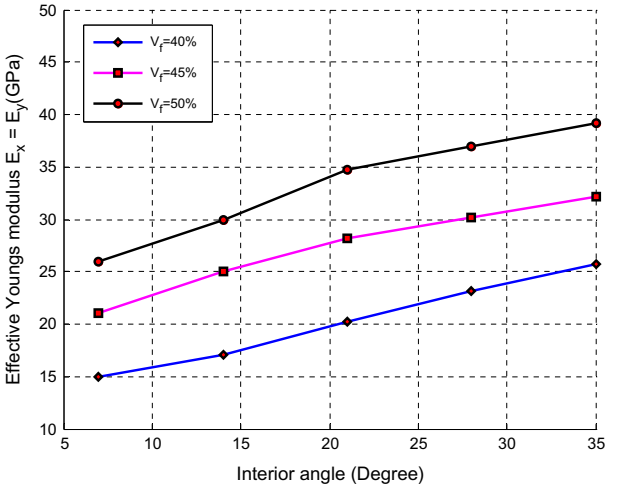

Figure 11. A plot of effective elastic modulus E_x and E_y ($E_x = E_y$) with interior angle.

(iii) Assume this effective properties as the equivalent matrix properties for the unit cell of 3-D full five-directional braided composite.
(iv) Take the properties of carbon fiber as reinforcement for the unit cell of 3-D full five-directional braided composite.
(v) Evaluate the effective properties of the CNT-based unit cell of 3-D full five-directional braided composite by applying the EMA and boundary conditions as presented in Table 2.

The second procedure to calculate the effective properties of CNT-based 3-D full five-directional braided composite is as follows (see Figure 14):

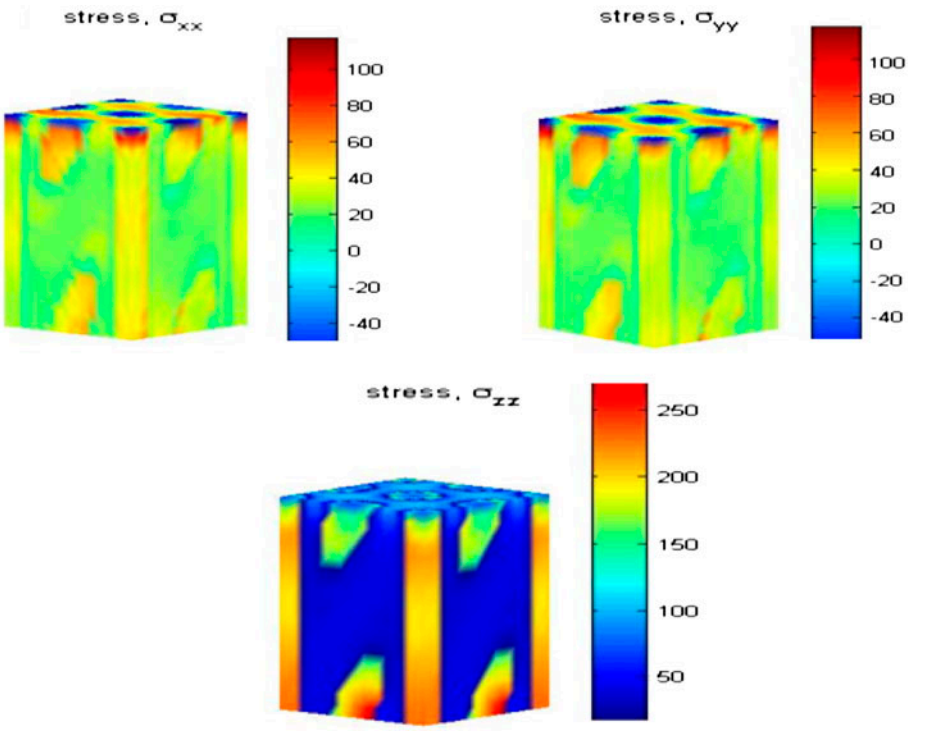

Figure 12. The plots of stress components σ_{xx}(MPa), σ_{yy}(MPa) and σ_{zz}(MPa) for the unit cell.

(a) Model the unit cell according to the given geometry of 3-D full five directional braided composite as shown in Figure 5.
(b) Generate the Gauss points.
(c) Calculate the total number of Gauss points in the unit cell and also identify the number of Gauss points in the matrix and fiber (axial and braiding yarns) individually; Randomly select 3% of total Gauss points in the matrix as:
    - 1% random in X_0 direction.
    - 1% random in Y_0 direction.
    - 1% random in Z_0 direction.
(d) Give 3% of Gauss points in the matrix region as CNTs properties and rest of the Gauss points in the matrix region as epoxy resin properties.
(e) Give the carbon fiber properties to those Gauss points which lie in the axial yarns and braiding yarns directions.
(f) Evaluate the effective properties of the CNT-based unit cell of 3-D full five-directional braided composite by applying the EMA and boundary conditions as shown in Table 2.

For both the procedures described above, the results are found nearly same. The first procedure looks more feasible to follow since whenever the matrix is required for further use, it can be directly applied in the model. Hence, in this study, the first procedure has been implemented to calculate the effective properties of 3-D full five-directional braided composite.

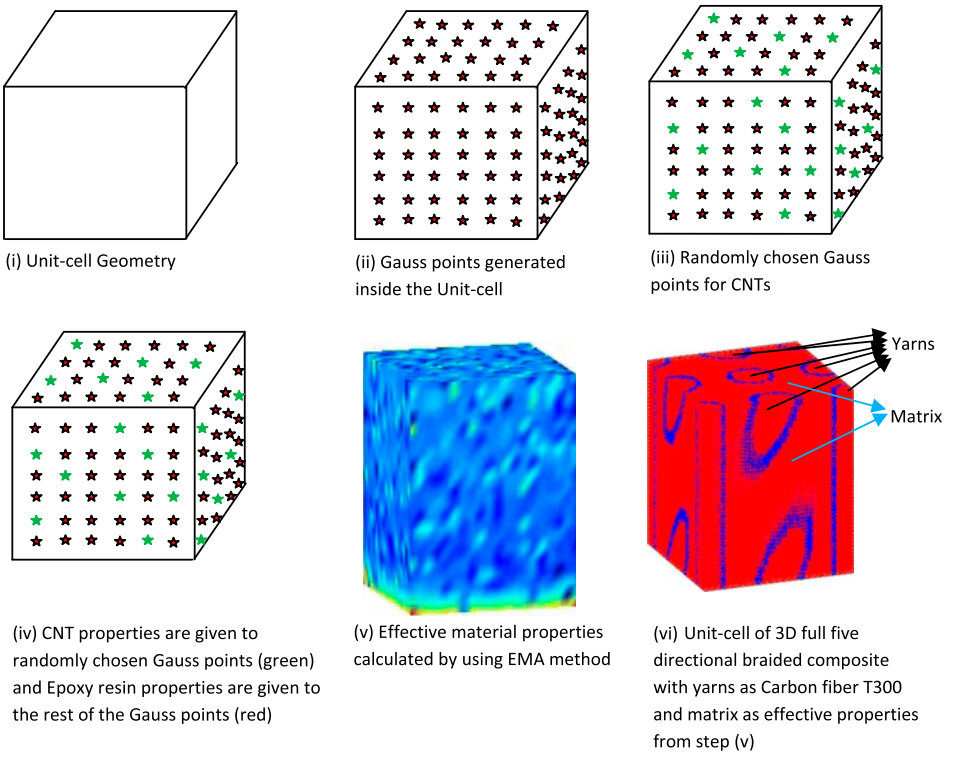

Figure 13. First procedure of modelling CNTs in the 3-D full five-directional braided composite.

5.1. *Implementation*

The XFEM has been used to analyze the proposed unit cell model. The dimensions of the unit cell are given in Table 6. This unit model is discretized by 6859 eight-nodded brick elements (8000 nodes). Total 54,872 Gauss points are generated. The elastic properties of matrix and fiber materials are listed in Table 7.

Three percentage (1% each is randomly distributed in X_0, Y_0, and Z_0 directions) of total Gauss points have been assigned the properties of reinforcement, i.e. CNT, whereas the rest of the Gauss points have been assigned the properties of matrix, i.e. epoxy resin.

After assigning the above mechanical properties to the constituents of the composite, the effective compliance matrix of the unit cell is found as:

$$S_{ij} = \begin{bmatrix} 0.0591 & -0.0177 & -0.0177 & 0 & 0 & 0 \\ -0.0177 & 0.0591 & -0.0177 & 0 & 0 & 0 \\ -0.0177 & -0.0177 & 0.0591 & 0 & 0 & 0 \\ 0 & 0 & 0 & 0.154 & 0 & 0 \\ 0 & 0 & 0 & 0 & 0.154 & 0 \\ 0 & 0 & 0 & 0 & 0 & 0.154 \end{bmatrix}_{GPa^{-1}} \tag{25}$$

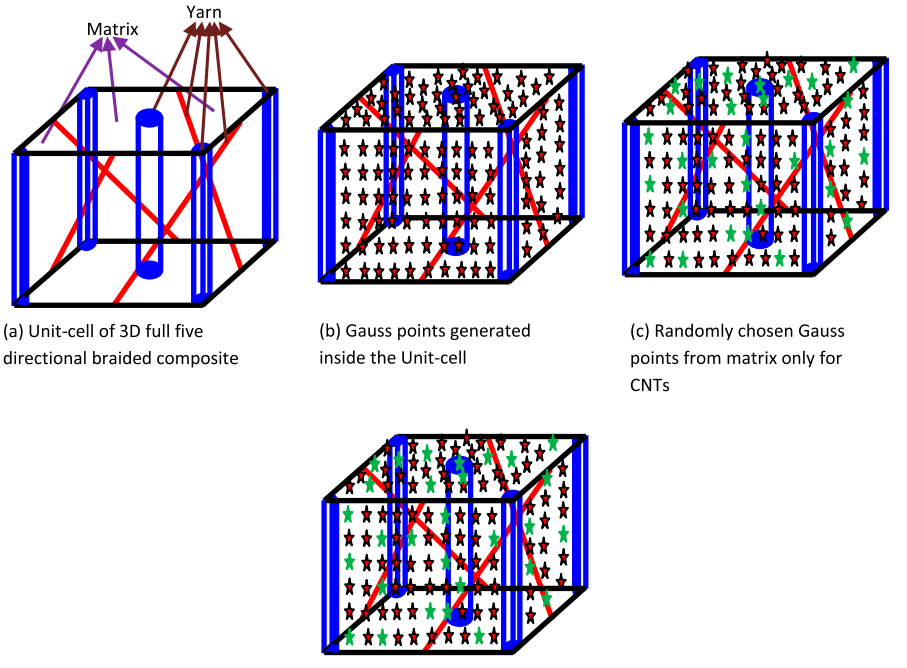

Figure 14. Second procedure of modelling CNTs in the 3-D full five-directional braided composite.

Table 6. Dimension of unit cell.

Parameters	Value (mm)
Width (a)	1
Thickness (b)	1
Height (c)	1

Table 7. Mechanical properties of component materials.

Materials	Young's mod ulus E_z (GPa)	Young's modulus $E_x = E_y$(GPa)	Poisson's ratio (v)
CNT	1000	100	0.3
Epoxy resin	4.5	4.5	0.3

According to the relationship among the engineering elastic constants and the compliance matrix S_{ij}, nine independent elastic constants of the unit cell are calculated and presented in Table 8.

According to first procedure of proposed CNT-based model, the properties presented in Table 8 will be used as the effective matrix properties for the simulation

Table 8. Effective elastic constants predicted by the model.

Young's modulus (GPa)			Shear modulus (GPa)			Poisson's ratio
E_x	E_y	E_z	G_{xy}	G_{yz}	G_{xz}	$v_{xz} = v_{yz} = v_{xy}$
16.9	16.9	16.9	6.5	6.5	6.5	0.3

of the braided composite in next step. In this step, the properties of fibers and matrix (obtained in first step) are used to evaluate the overall effective properties of 3-D full five-directional braided composite, as shown in Table 9.

After assigning the above mechanical properties to the components of the composite, the effective compliance matrix is evaluated by EMA using boundary conditions given in Tables 2 and 3 as:

$$S_{ij} = \begin{bmatrix} 0.0144 & -0.0043 & -0.0034 & 0 & 0 & 0 \\ -0.0043 & 0.0144 & -0.0034 & 0 & 0 & 0 \\ -0.0034 & -0.0034 & 0.0112 & 0 & 0 & 0 \\ 0 & 0 & 0 & 0.0338 & 0 & 0 \\ 0 & 0 & 0 & 0 & 0.0338 & 0 \\ 0 & 0 & 0 & 0 & 0 & 0.0375 \end{bmatrix}_{GPa^{-1}} \quad (26)$$

Using the relationship among the engineering elastic constants and the compliance matrix S_{ij}, the nine independent elastic constants of the unit cell are given in Table 10. Figure 15 shows a comparison of Young's modulus obtained with CNT and without CNT-based model, whereas Figure 16 shows a comparison of shear modulus with CNT and without CNT assuming same dimensions, fiber volume fraction, and interior angle of the unit cell. On the basis of these simulations, it is found that the braided composite with CNT has larger Young modulus and shear modulus than the braided composite without CNT.

Table 9. Mechanical properties of fiber and matrix materials.

Material	Young's modulus, E (GPa)	Poisson's ratio, v
Carbon fiber T300	221	0.3
Effective matrix properties (from Table 8)	16.9	0.3

Table 10. Comparison of the effective elastic constants with CNT and without CNTs.

Elastic constants	Without CNT (GPa)	With CNT (GPa)	Percentage increase
E_x	32.21	69.28	115.08
E_y	32.21	69.28	115.08
E_z	47.39	88.93	87.70
G_{xz}	14.60	29.55	95.54
G_{yz}	14.60	29.55	95.54
G_{xy}	12.39	26.64	115.06

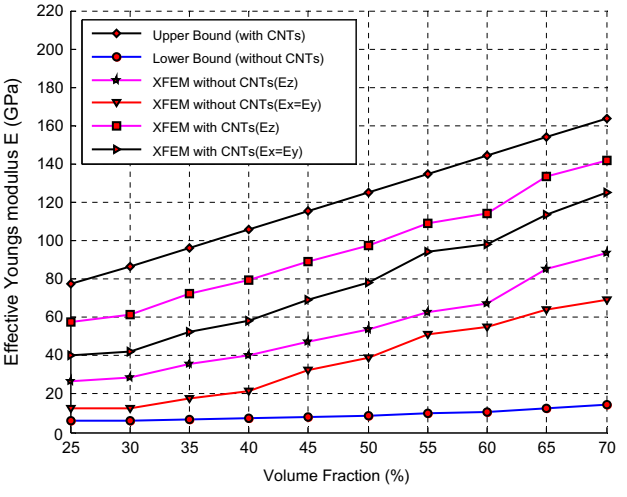

Figure 15. Comparison of the effective Young's modulus predicted by CNT-based model and without CNT-based model.

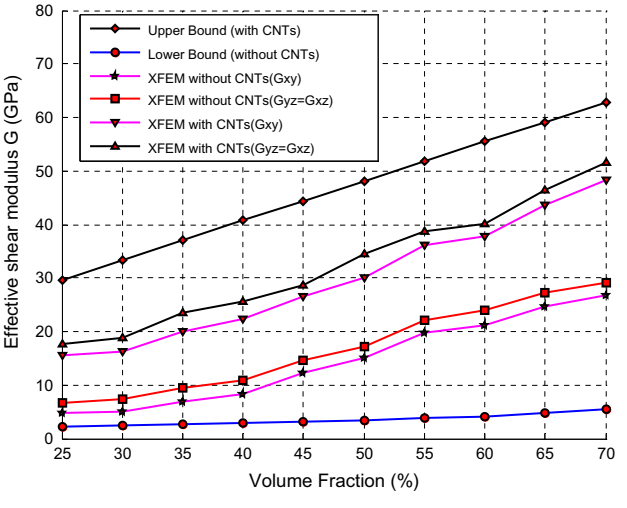

Figure 16. Comparison of the effective shear modulus predicted by CNT-based model and without CNT-based model.

6. Conclusion

In the present work, an extended finite element approach is used to evaluate the effective elastic properties of 3-D full five-directional braided composites. The present analysis takes into account the interaction among the fibers and matrix. The addition of CNT in the 3-D full five-directional braided composite leads to a significant improvement in the effective properties of the composite in all directions. These simulations show that the fiber volume fraction and interior angle affect the overall composite properties. Furthermore, the addition of 3% CNTs in composite enhances the elastic modulus nearly by 100%.

The proposed CNT-based unit cell model is easier to implement as compared to earlier CNT-based models as it does not require any modifications in conventional FEM/XFEM formulations. The effective mechanical properties of 3-D braided composites can be easily predicted by unit cell model for any combination of materials and volume fractions. In future, this work can be extended to perform the failure analysis of 3-D full five-directional braided composites.

References

[1] Mouritz AP, Bannister MK, Falzon PJ, Leong KH. Review of applications for advanced three-dimensional fibre textile composites. Compos. Part A. 1999;30:1445–1461.
[2] Li J, Jiao Y, Sun Y, Wei L. Experimental investigation of cut-edge effect on mechanical. Mater. Des. 2007;28:2417–2424.
[3] Fouinneteau MRC, Pickett AK. Shear mechanism modelling of heavy tow braided composites using a meso-mechanical damage model. Compos. Part A. 2007;38:2294–2306.
[4] Tao G, Liu Z, Lv M, Chen SS. Research on manufacture and test of advanced composite material flange. Open Mech. Eng. J. 2011;5:87–96.
[5] Li J. Three dimensional braiding composites for structural components. J. Spacecraft Recovery Remote Sens. 2007;28:53–58.
[6] Reese ED, Majidi AP, Pipes RB. Friction and wear behavior of fiber FP/aluminum composites. J. Reinf. Plast. Compos. 1988;7:500–514.
[7] Crane RM, Macander AB. Multidimensional braided fiber reinforced composite material characterization. Naval Eng. J. 1984;96:520–560.
[8] Sun X, Sun C. Mechanical properties of three-dimensional braided composites. Compos. Struct. 2004;65:485–492.
[9] Li D, Lu Z, Chen Li, Li J. Microstructure and mechanical properties of three-dimensional five-directional braided composites. Int. J. Solids Struct. 2009;46:3422–3432.
[10] Zeng T, Fang D, Guo LC, Ma L. A mechanical model of 3D braided composites with transverse and longitudinal cracks. Compos. Struct. 2005;69:117–125.
[11] Sun B, Liu F, Gu B. Influence of the strain rate on the uniaxial tensile behavior of 4-step 3D braided composites. Compos. Part A. 2005;36:1477–1485.
[12] Miravete A, Bielsa JM, Chiminelli A, Cuartero J, Serrano S, Tolosana N, de Villoria RG. 3D mesomechanical analysis of three-axial braided composite materials. Compos. Sci. Technol. 2006;66:2954–2964.
[13] Li D, Li J, Chen L, Lu Z, Fang D. Finite element analysis of mechanical properties of 3d four-directional rectangular braided composites part 1: microgeometry and 3d finite element model. Appl. Compos. Mater. 2010;17:373–387.
[14] Dong J, Feng M. Damage simulation for 3d braided composites by homogenization method. Chin. J. Aeronaut. 2010;23:677–685.
[15] Fang G, Liang J, Wang B. Progressive damage and nonlinear analysis of 3D four-directional braided composites under unidirectional tension. Compos. Struct. 2009;89:126–133.
[16] Xu K, Xu XW. Finite element analysis of mechanical properties of 3D five-directional braided composites. Mater. Sci. Eng. A. 2008;487:499–509.
[17] Li D, Fang D, Jiang N, Xuefeng Y. Finite element modeling of mechanical properties of 3-D five-directional rectangular braided composites. Compos. Eng. Part B. 2011;262:1359–8368.
[18] Zhang F, Liu Z, Wu Z, Tao G. A new scheme and micro-structural model for 3D full 5-directional braided composites. Chin. J. Aeronaut. 2010;23:61–67.
[19] Liu YJ, Chen XL, Belytschko T, Gu L. Evaluations of the effective material properties of carbon nanotube-based composites using a nanoscale representative volume element. Mech. Mater. 2003;35:69–81.
[20] Qian D, Dickey EC, Andrews R, Rantell T. Load transfer and deformation mechanisms in carbon nanotube-polystyrene composites. Appl. Phys. Lett. 2000;76:2868–2870.
[21] Sukumar N, Daux C, Moes N, Dolbow J, Belytschko T. Arbitrary branched and intersecting cracks with the extended finite element method. Int. J. Numer. Methods Eng. 2000;48:1741–1760.

[22] Singh IV, Mishra BK, Bhattacharya S, Patil RU. The numerical simulation of fatigue crack growth using extended finite element method. Int. J. Fatigue. 2012;36:109–119.
[23] Pathak H, Singh A, Singh IV. Numerical simulation of bi-material interfacial cracks using EFGM and XFEM. Int. J. Mech. Mater. Des. 2012;8:9–36.
[24] Chessa J, Smolinski P, Belytschko T. The extended finite element method (XFEM) for solidification problems. Int. J. Numer. Methods Eng. 2002;53:1959–1977.